

# **Modal analysis of broadband acoustic receptions at megameter ranges**

**Kathleen E. Wage, Arthur B. Baggeroer, and James C. Preisig**

March 2000

*Proceedings of the IEEE Sensor Array and Multichannel Signal  
Processing Workshop, pp. 102-106.*

© 2000 IEEE. Personal use of this material is permitted. However, permission to reprint/republish this material for advertising or promotional purposes or for creating new collective works for resale or redistribution to servers or lists, or to reuse any copyrighted component of this work in other works must be obtained from the IEEE.

# MODAL ANALYSIS OF BROADBAND ACOUSTIC RECEPTIONS AT MEGAMETER RANGES

Kathleen E. Wage

George Mason University  
MS 1G5, 4400 University Drive  
Fairfax, VA 22030  
kwage@gmu.edu

Arthur B. Baggeroer

Massachusetts Institute of Technology  
Rm 5-206, 77 Massachusetts Avenue  
Cambridge, MA 02139  
abb@arctic.mit.edu

James C. Preisig

Woods Hole Oceanographic Institution  
Bigelow 207, Mailstop #11  
Woods Hole, MA 02543  
jpreisig@whoi.edu

## ABSTRACT

*Normal modes, the eigenfunctions of the ocean waveguide, are useful in underwater acoustics because the lowest modes provide an efficient description of the most energetic signals at long ranges. Understanding the structure of the mode arrivals at megameter ranges is crucial to tomographic and matched field processing applications, but there have been few opportunities for experimental observations of these signals. This paper presents a short-time Fourier framework for broadband mode processing and applies it to data from the recent Acoustic Thermometry of Ocean Climate (ATOC) experiment. In doing so, this work explicitly addresses the issues associated with broadband signals that have been largely ignored in previous work and provides the first detailed analysis of the modal content of receptions at 3515 km range.*

## 1. INTRODUCTION

Normal modes are the eigenfunctions of the ocean waveguide, derived from the frequency-domain wave equation. They are useful in underwater acoustics, particularly in tomography and matched field processing, because the lowest modes provide an efficient description of the most energetic arrivals at long ranges. For example, Munk and Wunsch have proposed using very precise estimates of mode travel times and group velocities to invert for environmental parameters [1]. Using mode signals as observables requires the ability to associate an arrival with a particular path or section of the water column. In range-invariant environments, this problem is trivial because the modes propagate independently without exchanging energy, *i.e.*, an arrival in mode 1 is known to have traversed the entire path in mode 1. For a realistic ocean environment, however, inhomogeneities such as internal waves cause coupling of energy among the modes, making the problem much more difficult. Understanding the mechanisms and effects of mode coupling is crucial to using these signals in any type of application. While theoretical research has been done on long-range propagation of modes in deep water (*e.g.*, [2]), the Acoustic Thermometry of Ocean Climate (ATOC) experiment is one of the first opportunities to observe mode arrivals at megameter ranges. In this paper we develop a technique for estimating modal decompositions of broadband signals and use it to analyze receptions from the ATOC experiment.

This work was made possible by the experimental work carried out by the ATOC Group. The authors gratefully acknowledge support from the University of California-Scripps ATOC Agreement PO # 10037359 (a subcontract to the University of California) and Office of Naval Research Grant N00014-97-1-0788.

The modes are a frequency-dependent orthonormal basis in depth. Previous work on mode estimation has primarily focused on situations where a narrowband approximation is valid, *i.e.*, either the source is CW or the mode functions are approximately constant across the band of the source [3, 4]. A few researchers have implemented broadband mode processors using an FFT followed by narrowband estimation in each bin [5, 6, 7], but none have discussed the frequency resolution required for this method. We use a short-time Fourier transform approach to the broadband mode estimation problem because it provides a convenient framework for exploring time/frequency resolution tradeoffs. An important advantage of the STFT approach is that it allows us to study multiple arrivals within a single mode individually, rather than combining them by using a large FFT for the required frequency decomposition. It also is a natural way to measure the dispersion characteristics of the signals. Note that the algorithms described in previous work [5, 6, 7] fit within this general framework.

This paper presents results of the first detailed analysis of broadband mode arrivals at megameter range using data from the ATOC experiment. The focus is on using the STFT approach to process receptions for the 3515 km path from ATOC's source off the California coast to a receiving array near Hawaii.

The following section provides a brief overview of normal mode representations, using an ATOC example to highlight important characteristics (see references such as [8] for a detailed discussion of the theory). Section 3 presents the short-time Fourier framework for mode processing and discusses broadband performance issues. Finally, Section 4 describes some key results of the ATOC experimental data analysis.

## 2. NORMAL MODE REPRESENTATION

At each frequency, a mode is characterized by its wavenumber  $k_m$  and its modeshape  $\phi_m$ . For a given environment, defined by the sound speed profile and boundary conditions, the modes satisfy a second-order eigenvalue equation, *e.g.*, in cylindrical coordinates (assuming constant density):

$$\frac{d^2 \phi_m(r, z, \Omega)}{dz^2} + [k^2(r, z, \Omega) - k_m^2(r, \Omega)] \phi_m(r, z, \Omega) = 0. \quad (1)$$

In Eq. 1,  $\Omega$  is the temporal frequency, and  $k(r, z, \Omega)$  is the medium wavenumber as a function of range  $r$  and depth  $z$ . The modal wavenumber ( $k_m$ ) determines propagation characteristics, such as phase and group speeds, and the modeshape determines the spatial distribution of pressure due to each mode.

Since the modes are an orthonormal basis for narrowband signals, the acoustic pressure at coordinates  $(r, z)$  can be represented as the weighted sum

$$p(r, z, \Omega) = \sum_m a_m(r, \Omega) \phi_m(r, z, \Omega) \quad (2)$$

where  $a_m$  is the frequency-dependent coefficient for mode  $m$ . In general the sum in Eq. 2 is infinite, but in most realistic environments (such as the one considered in this paper) only a finite number of modes contribute to the field.

Figure 1 shows the sound speed profile and the first 10 modeshapes for the deep water environment at the ATOC Hawaii array. Note that each mode samples a different part of the waveguide:

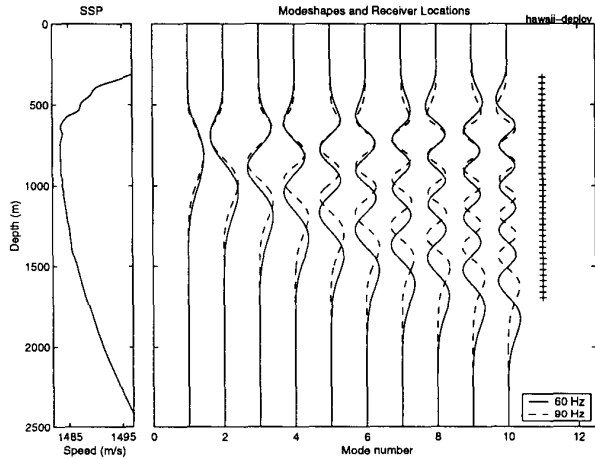


Figure 1: Sound speed profile and modeshapes (60 and 90 Hz) for the ATOC Hawaii environment. The +’s indicate nominal sensor positions for the 40-element array.

the lowest modes are concentrated around the sound speed minimum, while the higher modes span greater extents of the water column. As the plot indicates, the modes are functions of frequency. Over the 30 Hz interval shown (bandwidth of the ATOC source), the lowest modes change slightly, whereas the higher modes show significant variations in shape.

Figures 2 and 3 illustrate some relevant aspects of mode propagation in deep water. The top plot in Figure 2 shows a simulated time series generated using a deterministic range-varying model of the California-Hawaii ATOC path.<sup>1</sup> The spatial patterns associated with individual modes (*e.g.*, 5, 3, 2) are visible in the received pressure. Below the pressure plot is the modal time series obtained by projecting the field (finely sampled in depth) onto the mode functions at the receiver. The modes arrive in order from highest to lowest, as is consistent with deep water dispersion. Constructive interference of the higher modes result in the planewave (ray) arrivals in the early part of the reception. Figure 3 illustrates how the results change when the environment is perturbed by internal waves. Instead of a single, dispersive arrival in each mode, there are multiple arrivals. This “modal multipath” creates the more complicated interference patterns seen in the pressure time series.

<sup>1</sup>Parabolic equation simulation using sound speed profiles from the Levitus database.

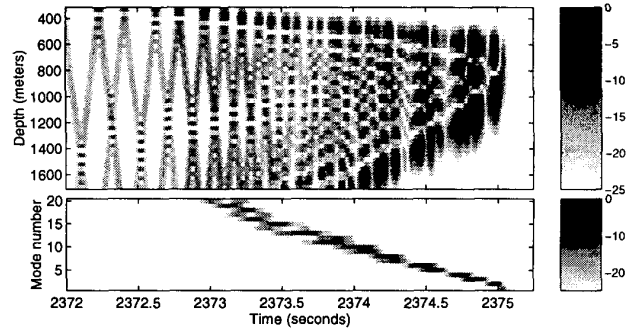


Figure 2: Deterministic, range-varying simulation for California-Hawaii ATOC path. Top panel shows the synthesized pressure field; bottom panel shows the corresponding time series for the first 20 modes.

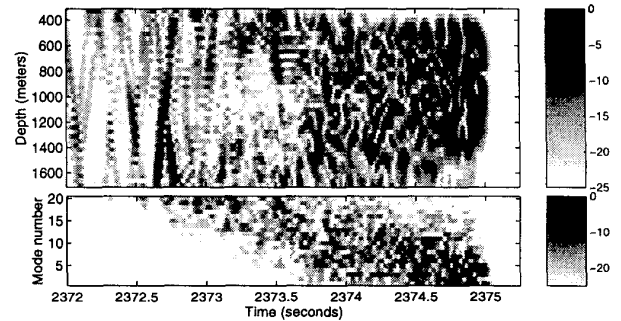


Figure 3: Simulation for California-Hawaii environment perturbed by internal waves (1/2 GM level). Top plot: pressure time series; bottom plot: modal time series.

### 3. SHORT-TIME FOURIER MODE PROCESSING

Since the modes vary as a function of frequency, processing must be done on a set of subbands to avoid mismatch problems. The short-time Fourier transform is a natural way to approach the frequency decomposition required in mode estimation. As Figure 4 illustrates, the STFT-based processor separates the received pressure into frequency bands using a filterbank (a set of complex demodulators cascaded with lowpass filters defined by  $H_{LP}[\omega]$ ). After filtering, the processor computes a vector time series of mode coefficients for each band using a set of narrowband modal beamformers. The outputs of the system are time-varying mode spectra that can be used to analyze the frequency-dependent structure in the signals, *e.g.*, dispersion. Within the STFT framework, the length of the lowpass filter,  $H_{LP}[\omega]$ , determines the time and frequency resolution of the estimates. Short filters are attractive because they have the potential to temporally resolve closely-spaced mode arrivals, but their wide passbands mean that the processor may be sensitive to the frequency-dependent variations of the modeshapes.

The STFT approach reduces the broadband estimation problem to a set of narrowband problems. Assuming that the modeshapes are constant over the band defined by the lowpass filter, the

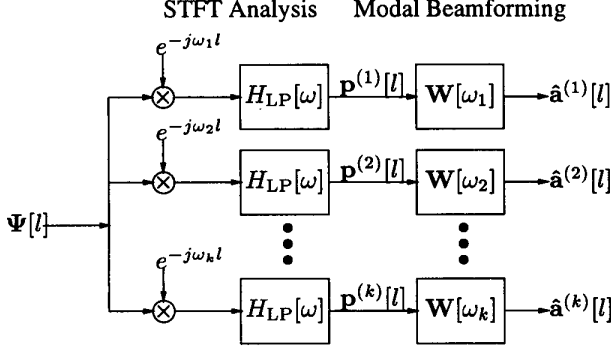


Figure 4: Block diagram of STFT-based mode processor

pressure measurement in the  $k$ th band becomes

$$\mathbf{p}^{(k)}[l] = \Phi[\omega_k] \mathbf{a}^{(k)}[l] + \mathbf{n}^{(k)}[l] \quad (3)$$

where  $\Phi$  is the matrix of sampled modeshapes,  $\mathbf{a}^{(k)}$  is a vector of time-varying mode coefficients and  $\mathbf{n}^{(k)}$  is a noise vector. Since little *a priori* information is available about the underlying modal time series, we restrict ourselves to mode estimates of the form:

$$\hat{\mathbf{a}}^{(k)}[l] = \mathbf{W}_k^H \mathbf{p}^{(k)}[l] \quad (4)$$

where  $\mathbf{W}_k^H$  is a matrix containing the deterministic, time-invariant spatial filter for the  $k$ th band. The next section briefly describes standard narrowband mode filters, and a subsequent section reviews their broadband performance.

### 3.1. Narrowband Mode Filters

Two standard solutions to the narrowband mode estimation problem are the matched filter [3] and the pseudo-inverse mode filter [4]. There are several ways to derive these filters. In this paper we briefly describe a constrained optimization approach that provides a complementary perspective to the estimation theory approach that is more common in the mode filtering literature (see [9] for a summary).

White noise gain,  $G_w$ , represents a convenient measure of processor sensitivity. For the mode processing problem, this quantity is defined for mode  $m$  as

$$G_w = N \frac{|\mathbf{w}_m^H \phi_m|^2}{\mathbf{w}_m^H \mathbf{w}_m \phi_m^H \phi_m}, \quad (5)$$

where  $\mathbf{w}_m$  is the weight vector (filter) and  $\phi_m$  is the sampled modeshape vector for the  $m$ th mode. Note that in deriving  $G_w$  we have used the arithmetic average SNR across the array as the input SNR (since SNR is not constant across the aperture). Applying the Schwartz inequality to Equation 5 demonstrates that the maximum value of the white noise gain is  $N$ , the number of sensors in the array.

The matched filter (MF) results from choosing the weight vector for mode  $m$  that maximizes white noise gain while maintaining a unit gain in the desired mode. Maximizing  $G_w$  subject to a unity gain constraint is mathematically equivalent to minimizing the squared length of the weight vector subject to the same gain constraint, thus the optimization problem becomes

$$\min \mathbf{w}_m^H \mathbf{w}_m \quad \text{subject to} \quad \mathbf{w}_m^H \phi_m = 1. \quad (6)$$

Standard optimization techniques yield the following solution for the weight matrix

$$\mathbf{W}^H = \begin{bmatrix} \frac{1}{\phi_1^H \phi_1} & & 0 \\ & \ddots & \\ 0 & & \frac{1}{\phi_M^H \phi_M} \end{bmatrix} \mathbf{E}^H \quad (7)$$

where  $\mathbf{E}$  is the sampled modeshape matrix containing the  $M$  desired modes, *i.e.*, the first  $M$  columns of  $\Phi$ . This filter is optimal in the sense that it achieves the maximum white noise gain ( $N$ ), but it does not explicitly prevent the signal in one mode from leaking into another. Instead, it relies on the orthogonality of the modes to separate them. It is important to note that while the modeshapes are orthogonal functions of the continuous variable  $z$ , the sampled modeshape vectors are not guaranteed to have this property.

The pseudo-inverse (PI) filter results from trying to constrain mode leakage by placing nulls in the modal beampattern at the locations of a set of interfering modes. In this case, the optimization problem consists of maximizing the white noise gain (minimizing the weight vector length) subject to multiple constraints, *i.e.*,

$$\min \mathbf{w}_m^H \mathbf{w}_m \quad \text{subject to} \quad \begin{cases} \mathbf{w}_m^H \phi_m = 1, \\ \mathbf{w}_m^H \phi_{n \neq m} = 0 \quad 1 \leq n \leq M. \end{cases} \quad (8)$$

Again standard optimization techniques yield a solution:

$$\mathbf{W}^H = (\mathbf{E}^H \mathbf{E})^{-1} \mathbf{E}^H. \quad (9)$$

Provided that the matrix  $\mathbf{E}$ , which contains a subset of the sampled modeshapes, has full rank, the null constraints are met exactly. White noise gain provides a convenient measure of the price paid for these nulls, and it is easy to show that  $G_w$  is directly connected with the conditioning of the pseudo-inverse.

### 3.2. Broadband Performance Analysis

In designing a short-time Fourier mode processor, it is crucial to have a measure of how well a narrowband mode filter designed for particular frequency performs on the modes at neighboring frequencies since this determines the required frequency resolution (and therefore the time resolution) of the lowpass filter. Figure 5 shows the matched filter and pseudo-inverse beampatterns as a function of frequency for modes 1 and 10, computed using the 40-element ATOC array shown in Figure 1. The pseudo-inverse filter includes the first 10 modes, which the array was designed to estimate. The solid lines in the figure represent the response in the desired mode and the dashed lines represent the crosstalk from neighboring modes (from 1 to 10) into the desired mode. At the design frequency (75 Hz), the pseudo-inverse filter clearly has nulls at the neighboring modes, while the matched filter does not. Both the MF and PI beampatterns indicate that crosstalk rejection is more significantly affected by frequency mismatch than is the response in the desired mode. Based on this plot and additional analysis in [10], these filters have an operating bandwidth of approximately  $\pm 2.5$  Hz.

Figure 6 is a plot of the white noise gain for modes 1 and 10 over the ATOC source band. The plots have 4 curves: one for the matched filter and three for different realizations of the pseudo-inverse filter that are designed for 10 modes, 12 modes, and 15 modes, respectively. Mode 1 is clearly unaffected by frequency, but conditioning problems are clearly evident for some of the mode 10 PI filters.

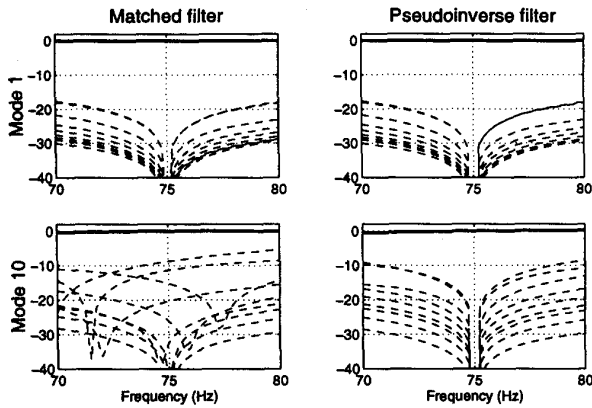


Figure 5: Frequency responses of the matched filter and pseudo-inverse mode filter for modes 1 and 10; filters designed for 75 Hz.

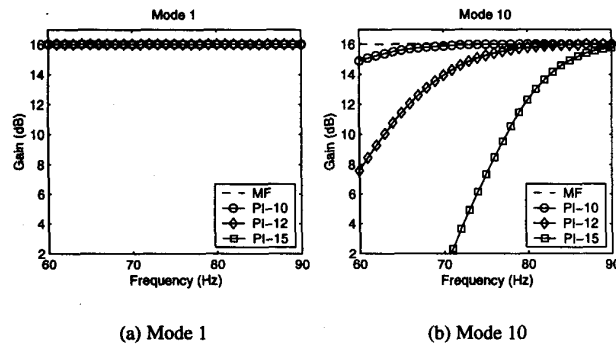


Figure 6: White noise gain as a function of frequency for the matched filter and three different pseudo-inverse filters (for 10 modes, 12 modes, and 15 modes).

For the experimental results presented in the following section, the STFT processor uses a pseudo-inverse filter for 10 modes in conjunction with an 0.4 second lowpass filter, which has the required  $\pm 2.5$  Hz bandwidth.

#### 4. EXPERIMENTAL RESULTS

The short-time Fourier approach described above has been used to analyze several months of data from the Acoustic Thermometry of Ocean Climate experiment carried out in 1996. The purpose of the ATOC experiment was to study long-range propagation of sound and to investigate acoustic methods for monitoring ocean climate variability. The acoustic network consisted of a broadband source off the California coast, two vertical line arrays (VLA's), and a number of bottom-mounted horizontal arrays. The source transmitted phase-encoded pseudo-random sequences that were demodulated, matched filtered, and averaged at the receiver. This paper focuses on analysis of receptions from the 40-element array located near Hawaii, at a range of 3515 km from the source.

#### 4.1. Processing Example

Figure 7 shows a reception on the Hawaii VLA, and Figure 8 shows the corresponding mode estimates. These plots reveal im-

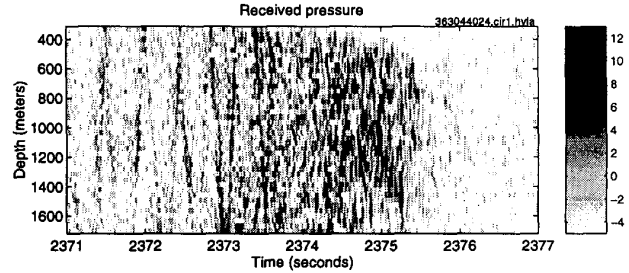


Figure 7: Reception on 40-element ATOC VLA at Hawaii

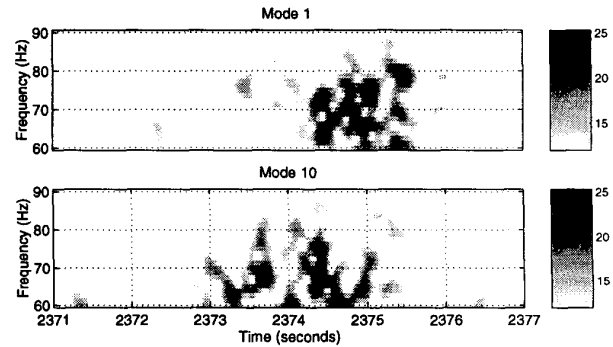


Figure 8: Frequency-stacked estimates for modes 1 and 10

portant features of the mode signals at megameter range. First, each low mode contains series of arrivals, rather than the single dispersive arrival that would characterize adiabatic (no coupling) propagation. The mode estimates show frequency-selective fading due to destructive interference of overlapping multipaths, suggesting that the STFT processor is not temporally resolving all of the arrivals. Despite the complexity of the signals, it is important to note that some deep water dispersion characteristics are still evident, *i.e.*, the mean arrival time of mode 10 appears to be less than that of mode 1.

#### 4.2. Statistics

The complicated multipath arrival structure at 3515 km exhibits significant temporal variability: average coherence times are on the order of 6-8 minutes [10]. Given the amount of fluctuation observed on time scales of minutes, it is clear that transmissions at four-hour intervals essentially measure different realizations of the internal wave field. A statistical analysis of groups of receptions has shown that modes do retain travel-time information at megameter ranges. As an example, consider the average mode arrival times shown in the top plot of Figure 9. The data points correspond to the centroids of the mode signals as a function of frequency averaged over 4 days worth of receptions. These centroids show the expected dispersion characteristics of a deep water channel, *i.e.*,

high modes arriving first; low modes arriving last. In addition, there is a slight trend across frequency for the highest modes: the higher frequencies arrive later, as expected in deep water. Further

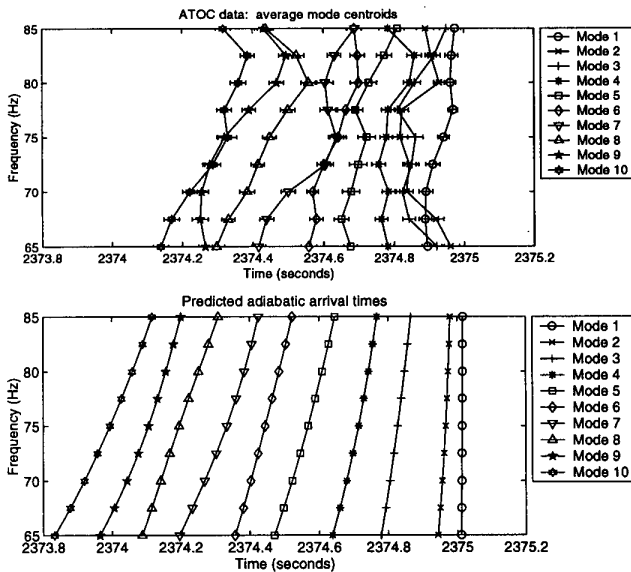


Figure 9: Comparison of average mode arrival times for a group of ATOC receptions and adiabatic arrival time predictions

analysis of the centroid data has shown that there are statistically significant trends in mode arrival time over the course of 5 months. Figure 10 shows the average arrival times in the 75 Hz bin as a function of yearday. These observed trends in the late arrivals agree with results from a planewave analysis of the earliest arrivals in the ATOC receptions [11].

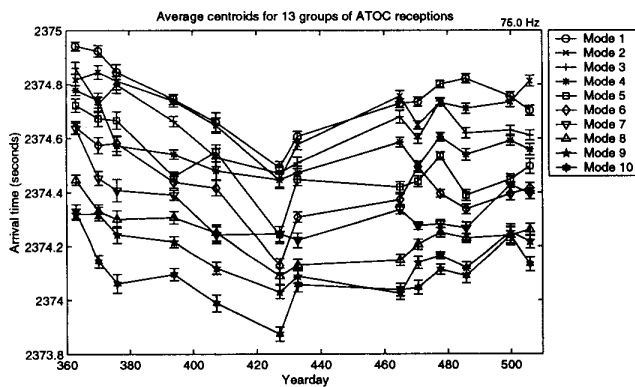


Figure 10: Centroids in 75 Hz bin as a function of yearday

## 5. REFERENCES

[1] W. Munk and C. Wunsch, "Ocean acoustic tomography: Rays and modes," *Reviews of Geophysics and Space Physics*,

vol. 21, pp. 777–793, May 1983.

- [2] L. Dozier and F. Tappert, "Statistics of normal mode amplitudes in a random ocean. I. Theory," *J. of the Acoustical Society of America*, vol. 63, pp. 353–365, February 1978.
- [3] R. H. Ferris, "Comparison of measured and calculated normal-mode amplitude functions for acoustic waves in shallow water," *J. of the Acoustical Society of America*, vol. 52, no. 3, pp. 981–988, 1972.
- [4] C. Tindle, K. Guthrie, G. Bold, M. Johns, D. Jones, K. Dixon, and T. Birdsall, "Measurements of the frequency dependence of normal modes," *J. of the Acoustical Society of America*, vol. 64, pp. 1178–1185, October 1978.
- [5] T. Yang, "Broadband source localization and signature estimation," *J. of the Acoustical Society of America*, vol. 93, pp. 1797–1806, April 1993.
- [6] P. Sutton, W. Morawitz, B. Cornuelle, G. Masters, and P. Worcester, "Incorporation of acoustic normal mode data into tomographic inversions in the Greenland Sea," *J. of Physical Oceanography*, vol. 99, pp. 12487–12502, June 1994.
- [7] K. D. Heaney and W. Kuperman, "Very long-range source localization with a small vertical array," *J. of the Acoustical Society of America*, vol. 104, pp. 2149–2159, October 1998.
- [8] L. Brekhovskikh and Y. Lysanov, *Fundamentals of Ocean Acoustics*. New York, NY: Springer-Verlag, 2nd ed., 1991.
- [9] J. R. Buck, J. C. Preisig, and K. E. Wage, "A unified framework for mode filtering and the maximum *a posteriori* mode filter," *J. of the Acoustical Society of America*, vol. 103, pp. 1813–1824, April 1998.
- [10] K. E. Wage, *Broadband Modal Coherence and Beamforming at Megameter Ranges*. PhD thesis, Massachusetts Institute of Technology/Woods Hole Oceanographic Institution, February 2000.
- [11] The ATOC Consortium, "Ocean Climate Change: Comparison of Acoustic Tomography, Satellite Altimetry, and Modeling," *Science*, vol. 281, pp. 1327–1332, August 28 1998.